Massive Stars: Feedback Effects in the Local Universe

By M. S. OEY[1] AND C. J. CLARKE[2]

[1]Department of Astronomy, 830 Dennison Building, University of Michigan, Ann Arbor, MI 48109-1042, USA

[2]Institute of Astronomy, University of Cambridge, Madingley Road, Cambridge CB3 0HA, UK

Massive stars as a population are the source of various feedback effects that critically impact the evolution of their host galaxies. We examine parameterizations of the high-mass stellar population and self-consistent parameterizations of the resulting feedback effects, including mechanical feedback, radiative feedback, and chemical feedback, as we understand them in the local universe. To date, it appears that the massive star population follows a simple power-law clustering law that extends down to individual field massive stars, and the robust stellar IMF appears to have a constant upper-mass limit. These properties result in specific patterns in the HII region luminosity function, and the ionization of the diffuse, warm ionized medium. The resulting supernovae generate a population of superbubbles whose distributions in size and expansion velocity are also described by simple power laws, and from which a galaxy's porosity parameter is easily derived. A critical star-formation threshold can then be estimated, above which the escape of Lyman continuum photons, hot gas, and nucleosynthetic products is predicted. A first comparison with a large sample of Hα observations of galaxies is broadly consistent with this prediction, and suggests that ionizing photons are likely to escape from starburst galaxies. The superbubble size distribution also offers a basis for a Simple Inhomogeneous Model for galactic chemical evolution, which is especially applicable to metal-poor systems and instantaneous metallicity distributions. This model offers an alternative interpretation of the Galactic halo metallicity distribution and emphasizes the relative importance of star-formation intensity, in addition to age, in a system's evolution. The fraction of zero-metallicity, Population III stars is easily predicted for any such model. We emphasize that all these phenomena can be modeled in a simple, analytic framework over an extreme range in scale, offering powerful tools for understanding the role of massive stars in the cosmos.

1. Introduction

Massive stars are of great interest because of their profound feedback effects that alter the surrounding environment on local, global, and cosmic scales. Their radiative feedback causes ionization of neutral gas; their supernova (SN) explosions drive mechanical feedback that shock-heats gas to $\gtrsim 10^6$ K; and the nucleosynthesis processes within these stars and their SNe produce most of the elements that are tracers of past stellar populations. In short, massive stars are one of the principal drivers of galactic and cosmic evolution.

2. The Massive Star Population

By "massive stars," we consider those stars having masses above, say, 10 $M_\odot$. If we are to understand the global feedback effects from massive stars, then it is important to understand their properties as a *population*. This population of stars is characterized by its distribution in (a) mass, and (b) space.

FIGURE 1. Three-color image of the R136a cluster in 30 Doradus, imaged with the NTT. Red, green, and blue correspond to V, B, and U, respectively. (From Selman et al. 1999*a*.)

2.1. *The IMF and Upper-Mass Limit*

The stellar mass distribution is parameterized by the familiar stellar initial mass function (IMF). The massive star IMF has been evaluated many times for OB associations and clusters in the Galaxy and Magellanic Clouds (e.g., Massey 2003), and it appears to be fairly robustly consistent with the Salpeter (1955) slope:

$$n(m)\ dm \propto m^{-2.35}\ dm \tag{2.1}$$

where $n(m)$ is the number of stars in the mass range m to $m+dm$. Cruder evaluations of extragalactic massive star populations using integrated colors and properties of galaxies support this result (e.g., Elmegreen 2006; Fernandes *et al.* 2004; Bell & de Jong 2001; Baldry & Glazebrook 2003). An important possible exception may be the field massive star IMF (see below). Beware, however, that it is difficult to disentangle effects of the IMF slope and upper-mass cutoff.

While the slope of the upper IMF is fairly well-determined, the upper-mass limit is less so. There are theoretical considerations supporting the existence of a stellar upper-mass limit based on physical instability arguments (e.g. Ledoux 1941; Schwarzschild & Härm 1958; Stothers 1992), as well as limitations related to the high rate and short timescales of accretion that are needed to overcome the protostar's own radiation pressure (e.g. Larson

& Starrfield 1971; Kahn 1974; Elmegreen & Lada 1977; Wolfire & Cassinelli 1987; Bonnell, Bate, & Zinnecker 1998). These issues are also discussed elsewhere in these Proceedings (e.g., reviews by Krumholz and Bonnell). While the physical processes remain to be fully understood, we can in the meantime empirically evaluate the upper-mass limit, or lack thereof.

The IMF dictates that the highest-mass stars are the rarest, and so the obvious place to search for such stars is in the richest clusters that are young enough ($\lesssim 3$ Myr) to preclude any having exploded as SNe. These rich, extremely young clusters are likewise rare (see below), but we are fortunate that local examples do exist. The R136a cluster in the 30 Doradus star-forming complex in the Large Magellanic Cloud (LMC; Figure 1) is one such example. Selman et al. (1999*b*) examined this region using extensive ground-based observations and suggested that R136a exhibits an upper-mass cutoff around 150 $M_\odot$, based on fairly qualitative arguments. Massey & Hunter (1998) and Hunter et al. (1997) evaluated zero-age main sequence (ZAMS) masses of hundreds of the most massive stellar candidates in R136a, based on photometry and spectroscopic classifications from *HST*. Weidner & Kroupa (2004) and Oey & Clarke (2005) both examined the Massey & Hunter statistics of these reported data for R136a and independently concluded that this region quantitatively demonstrates an upper-mass limit around $150-200$ $M_\odot$. Another example of an extremely young and extremely rich cluster is the Arches Cluster in the Galactic center environment. It, too, exhibits an upper-mass limit around $150-200$ $M_\odot$ (Figer 2005).

But R136a and the Arches Cluster are only two specific regions. Since star formation presumably is a stochastic process, it may be that we were simply extremely unlucky to have picked two clusters that both happened to have rendered unusually low maximum stellar masses, even though the physical mass limit may be much higher. Furthermore, only one or two more examples of rich clusters suitable for deterministic evaluation of an upper-mass limit may be accessible for such detailed, empirical, stellar mass analyses. However, *if* the IMF indeed behaves like a universal probability density function (PDF), then we can also use a combined ensemble of the stellar contents of the numerous, ordinary OB associations to evaluate an upper-mass limit. Note that such treatment of the IMF as a PDF is indeed the conventional way in which it is usually considered.

We can then assemble a large number of the youngest massive stars and examine the form of the upper IMF. For a Salpeter IMF, we can write the expectation value of the maximum stellar mass $m_{\rm max}$ for an ensemble of N_* stars having masses $m \geqslant 10$ $M_\odot$, given a physical upper-mass limit $m_{\rm up}$:

$$\langle m_{\rm max} \rangle = m_{\rm up} - \int_0^{m_{\rm up}} \left[\int_0^M \phi(m)\ dm \right]^N dM \quad , \tag{2.2}$$

where $\phi(m)$ is the IMF. Oey & Clarke (2005) considered data for 8 OB associations in the Galaxy and LMC in which the upper IMF was fully evaluated by Massey et al. (1995), based on spectroscopic classifications, and which they found to be $\leqslant 3$ Myr old. Among these associations, there is a total of 263 stars having $m \geqslant 10$ $M_\odot$. For a physical $m_{\rm up}= 1000$ $M_\odot$, equation 2.2 predicts an expected $m_{\rm max}> 450$ $M_\odot$ (Figure 2), whereas the observed maximum mass is $\lesssim 150$ $M_\odot$. Since R136a was studied by the same group, we can include it in this uniform sample, raising the total number to 913 stars having $m \geqslant 10$ $M_\odot$. For the same parent IMF assumptions, Figure 2 shows that the predicted $m_{\rm max}$ is now ~ 600 $M_\odot$. However, the observed maximum stellar mass in the entire ensemble is still only around 150 $M_\odot$, and so Figure 2 implies a similar physical upper-mass cutoff.

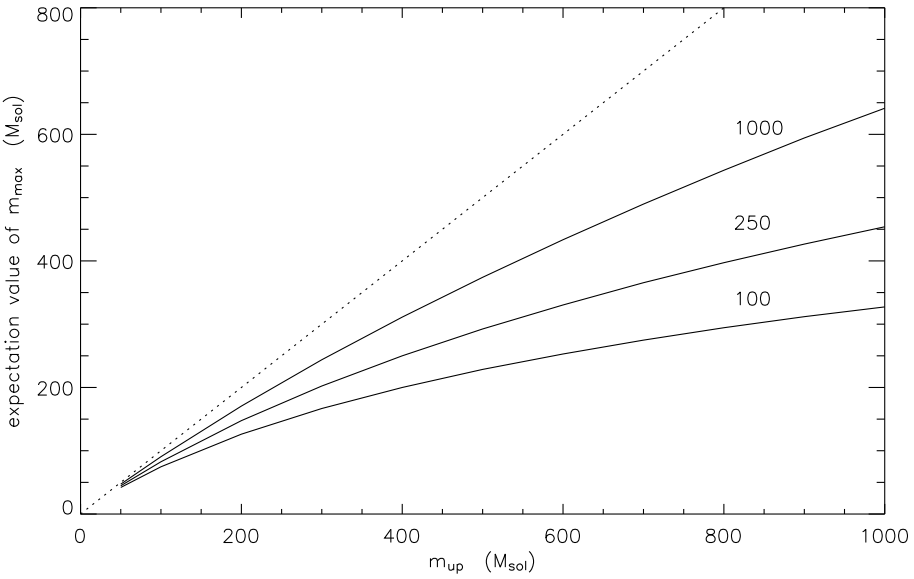

FIGURE 2. Expectation value of the maximum mass star in a cluster, given N stars having $m \geqslant 10$ $M_\odot$, as a function of physical upper mass limit $m_{\rm up}$. (From Oey & Clarke 2005.)

Once again, we could be exceedingly unlucky in considering an extraordinary sample of 9 associations, all of which happened to render an unusually low $m_{\rm max}$. Oey & Clarke (2005) quantified the likelihood of this occurrence as well, for physical $m_{\rm up}$ ranging from ∞ to 120 $M_\odot$. Only $m_{\rm up} \sim 120-150$ $M_\odot$ yielded significant probabilities for the observed $m_{\rm max}$ in the individual clusters simultaneously, therefore clearly demonstrating an upper-mass cutoff around those values. Koen (2006) used an alternative statistical analysis with these same data that confirms this result.

Clearly, this upper-mass limit is only demonstrated for this particular sample of objects, and assuming that they are all pre-SN. It seems significant, however, that the *same* $m_{\rm up}$ is found across grossly varying environments encompassing the extreme conditions near the Galactic Center for the Arches Cluster; the highly-active, yet much less extreme conditions for R136a; and the relatively unremarkable conditions for the OB associations. These findings suggest a universal upper-mass limit around 150 $M_\odot$ in the local universe. Elmegreen (2000; 2006) makes similar arguments in considering aggregrate stellar populations of galaxies.

2.2. *The Clustering Law*

With a fairly well-defined parameterization of the stellar mass distribution for the upper IMF, we now turn to the spatial distribution of the massive star population. We can parameterize the space distribution by defining a *clustering law*, $N(N_*)$, which describes the distribution in N_*, the number of massive stars per cluster. Over the last decade, it has become apparent that the clustering law for young, massive clusters is robustly consistent with a power-law, similar to the stellar IMF:

$$N(N_*)\, dN_* \propto N_*^{-2}\, dN_* \quad . \tag{2.3}$$

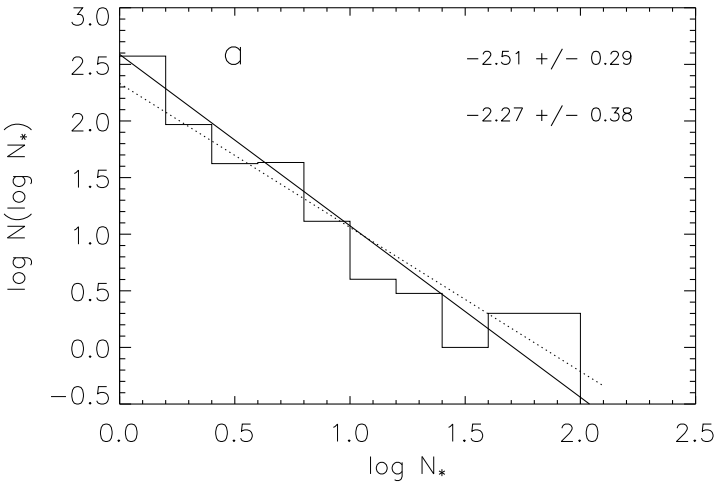

FIGURE 3. SMC clustering law for OB star candidates, from Oey et al. (2004). The solid line shows a fit to the entire dataset, while the dotted line shows a fit omitting the field stars (first bin, at $\log N_* = 0$). These fitted slope values are shown, respectively.

This is equivalent to the initial cluster mass function and is seen in a variety of environments, including starbursts and populations of super star clusters (e.g., Meurer et al. 1995; Zhang & Fall 1999) and extrapolated from the globular cluster present-day mass function (e.g. Elmegreen & Efremov 1997; Hunter et al. 2003).

The upper-mass cutoff to the clustering law appears to vary in different systems (see below), but no physical maximum has yet been suggested. In the opposite, low-mass extreme, the "clusters" reduce to single, individual field massive stars. With the definition of "massive" stars as above, "field" massive stars include both those that are genuinely isolated from any other stars, if they exist, and those that are the "tip of the iceberg" for a small group whose remaining members all have m less than would qualify for our definition of a "massive" star.

What is the relationship between the field massive stars and those in clusters? Oey et al. (2004) studied a uniformly selected sample of massive star candidates from $UBVR$ photometry (Massey et al. 2002) and recalibrated FUV $B5$ (Parker et al. 1998) photometry across most of the Small Magellanic Cloud (SMC) and determined the clustering law using a friends-of-friends algorithm. For that galaxy, they found that the massive star clustering follows a smooth power law all the way down to $N_* = 1$, and that the power-law exponent is consistent with equation 2.3 (Figure 3).

At face value, this suggests the co-existence of a universal IMF and universal clustering law, of the respective forms in equations 2.1 and 2.3. However, we caution that the field star IMF has been suggested to be significantly steeper than in clusters, based on both observations (Massey 2002) and theoretical arguments (Kroupa & Weidner 2003). If this is indeed the case, then a flattening should be observed in the clustering law near $N_* = 1$, since this implies fewer field stars. Because this flattening is not observed in Figure 3, there must be a corresponding steepening in the clustering law in this regime, in order to recover the smooth power law that we see in the SMC data. Thus reality may be

somewhat subtle and more complex than is seen at face value; Oey et al. (2004) discuss this issue in more detail.

Regardless of any underlying complexities, the resulting observed clustering law in the SMC does show a smooth power law described by equation 2.3. If this applies generally, then we can directly estimate the fraction of field massive stars as (Oey et al. 2004):

$$f_{\rm field} = \left(\ln N_{*,\rm max} + 0.5772\right)^{-1} \quad , \tag{2.4}$$

where $N_{*,\rm max}$ is the number of massive stars in the richest cluster of the ensemble. Because of this dependence on $N_{*,\rm max}$, we see that the field star fraction has a modest inverse dependence on the total star formation rate of the system. For typical star-forming galaxies, $f_{\rm field} \sim 20 - 25\%$.

The preceding thus describes a well-defined parameterization for the massive star population in star-forming galaxies, given by equations 2.1 and 2.3, and adopting a stellar upper-mass cutoff $m_{\rm up}$= 150 $\rm M_\odot$.

3. Radiative Feedback

Now turning to the feedback effects from this massive star population, we begin by considering the radiative feedback, which refers to the photoionization caused by these stars. There are two principal effects: the generation of ordinary HII regions, and the generation of the diffuse, nebular component of the interstellar medium (ISM). The latter is usually referred to as the warm ionized medium (WIM), or alternatively, diffuse ionized gas (DIG).

3.1. *The* HII *Region Luminosity Function*

The Hα luminosity is a direct probe of the cumulative massive star population in an HII region, and the clustering law naturally results in a corresponding power-law luminosity function for the classical HII regions, which has been empirically examined in many nearby galaxies. However, the HII region luminosity function (HIILF) is often seen to deviate from a smooth N_*^{-2} power law in the following ways: (1) a two-slope form is often seen, with the lower-luminosity population showing a shallower power-law slope; (2) inter-arm nebular populations in grand design spirals often show shallower slopes than the arm populations; and (3) there is a correlation with galaxy type, such that the early-type galaxies show much steeper slopes than late types. Oey & Clarke (1998*a*) demonstrated, using Monte Carlo models, that these variations are all fully consistent with, and indeed expected, from the properties of the massive star population described above. One of the most important effects is a flattening that is seen in the HIILF at low luminosities, that results from stochastic sampling of the stellar IMF in this "unsaturated" regime (Figure 4). For luminous nebulae generated by rich, "saturated" clusters that fully sample the IMF through the upper-mass limit $m_{\rm up}$, the HII region luminosity is directly proportional to N_*; whereas for sparse, "unsaturated" clusters, the resulting HII region luminosity is subject to the specific stellar population. The stochastic flattening in the low-luminosity end of the HIILF quantitatively explains the observed effects (1) and (2) described above. The second of these, the observed steepening seen for inter-arm HII regions, can be explained if these show an evolved slope as in Figure 4*b*, while the zero-age population in the arms corresponds to the model in Figure 4*a*. As a single-age population evolves, the entire distribution fades, and the low-luminosity regime becomes dominated by evolved saturated objects. Oey & Clarke (1998*a*) demonstrate this effect in nearby grand-design spirals, where the inter-arm regions are presumably a more evolved population left behind in the wake of the spiral density waves.

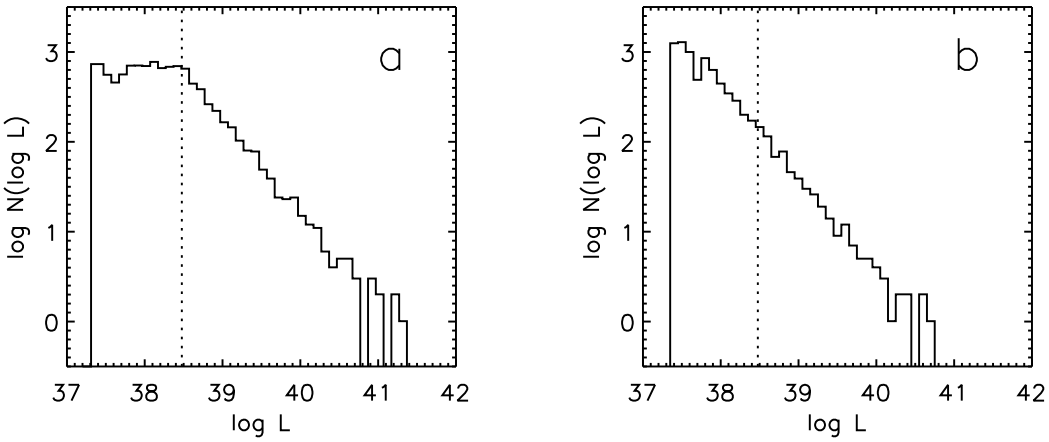

FIGURE 4. Monte Carlo models of the zero-age HII region luminosity function (panel *a*) and the same distribution evolved to 7 Myr (panel *b*). The dotted lines show the Hα luminosity associated with the most massive star in the IMF. (From Oey & Clarke 1998*a*.)

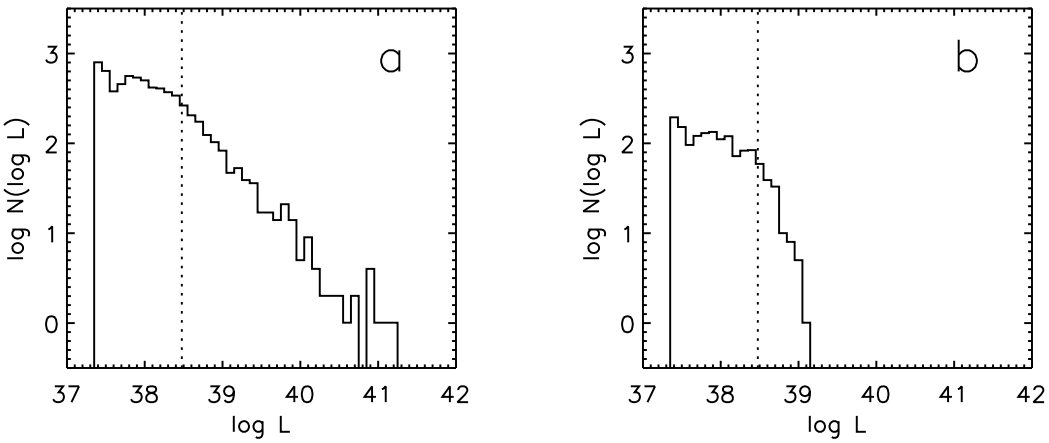

FIGURE 5. Monte Carlo models of the HII region luminosity function for continous star formation. Panel *a* shows the distribution for no upper-mass limit to the clusters, and panel *b* shows the same, but imposing a limit of $N_* = 10$. (From Oey & Clarke 1998*a*.)

The third effect, the trend with galaxy Hubble type, can be explained by a varying upper cutoff in N_*, while preserving the –2 power-law slope. Figure 5*a* shows a Monte Carlo model with no upper-mass limit to the clusters, while Figure 5*b* shows the same model HIILF, but imposing a limit of $N_* \leqslant 10$. The former are qualitatively and quantitatively similar to the observed HIILF in late-type galaxies (e.g., Kennicutt et al. 1989; Rand 1992; Banfi et al. 1993; Rozas et al. 1996) while the former agree with the observations for Sa galaxies (Caldwell et al. 1989) Thus, all three of the observed patterns in the HIILF are fully consistent with, and indeed expected, for the universal clustering law. Oey & Clarke (1998*a*) describe these phenomena in detail.

3.2. *The Diffuse, Warm Ionized Medium*

Classical HII regions account for only about half of the total Hα emission from star-forming galaxies (e.g., Walterbos 1998; Ferguson et al. 1996). The remaining half originates from the widespread, diffuse WIM. While the ionization of the WIM remains to be fully understood, it generally thought also to originate from massive stars (e.g., Reynolds 1984). Direct comparisons of the stellar populations in LMC OB associations with their associated nebular luminosities suggests that up to 50%, and in some cases, more, of the ionizing radiation could escape from HII regions (Oey & Kennicutt 1997; Voges et al. 2005). Hoopes & Walterbos (2003) came to a similar conclusion based on FUV observations of M33 from *UIT*.

The other half of WIM ionization can be accounted for by field stars, assuming that the universal clustering law indeed extends to individual massive stars representing the "tip of the iceberg" on sparse clusters and groups, as found above for the SMC. Equation 2.4 predicts that typically about 25% of the massive star population resides in the field as defined in this way, a fraction confirmed empirically for the SMC (Oey et al. 2004). Thus, field stars can account for one-quarter of a galaxy's total Hα luminosity. For the WIM constituting half of that total, then the field stars can ionize about half again of the WIM.

There are a few caveats; for example, other ionization processes are implicated by apparent detailed ionization states observed in the WIM (e.g. Reynolds *et al.* 1999; Rand 2000). Also, the most recent hot star atmosphere models (e.g. Martins et al. 2005; Repolust et al. 2005; Smith et al. 2002) are suggesting softer ionizing fluxes which may reduce the role of massive stars. However, it seems clear that this stellar population dominates production of the WIM.

Radiative feedback to the IGM is also a topic of vital current interest, and is discussed further below.

4. Mechanical Feedback

We now turn to the mechanical energy produced by the core-collapse supernovae of the massive star population. Given the short ($\leqslant$ 40 Myr) lifetimes of these stars, the overwhelming majority remain in the OB associations where they were born, and so the subsequent SNe are spatially clustered. Our universal N_*^{-2} clustering law translates directly into a mechanical luminosity function, that parameterizes the kinetic energy for the ensemble of clusters. Assuming that all SNe yield the same kinetic energy, we can write the mechanical luminosity function as

$$N(L)\ dL \propto L^{-2}\ dL \quad , \tag{4.1}$$

where L is the "mechanical luminosity" or SN power expected from a given cluster. This makes the rough approximation that the discrete SNe represent a continuous energy input over the 40 Myr timescale (e.g., McCray & Kafatos 1987).

4.1. *Superbubbles in the ISM*

The evolution of multi-SN superbubbles is given by simple, Sedov-like relations (e.g., Weaver et al. 1977):

$$R \propto \left(L/n\right)^{1/5}\ t^{2/5} \tag{4.2}$$

$$P_i \propto L^{2/5}\ n^{3/5}\ t^{-2/5} \quad , \tag{4.3}$$

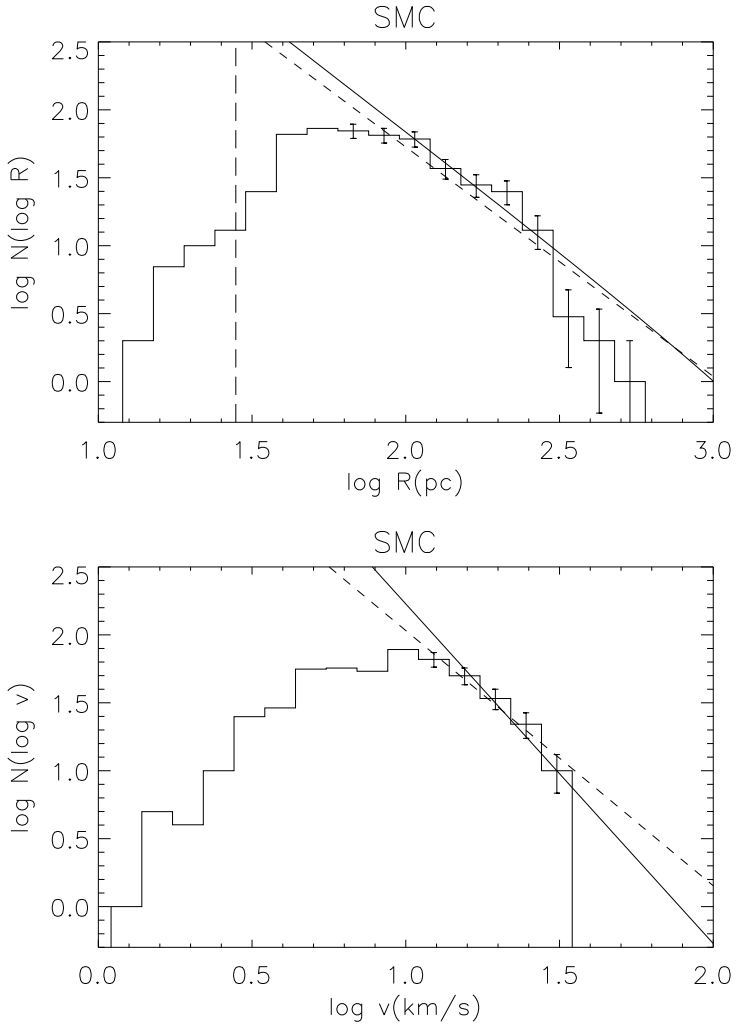

FIGURE 6. SMC HI shell size distribution (top) and expansion velocity distribution (bottom) from the survey by Staveley-Smith *et al.* (1997). The overplotted lines in the top panel show a power-law fit of 2.7 ± 0.6 to the data (dashed), and a slope of 2.8 ± 0.4 (solid) predicted from the observed HIILF for this galaxy. The spatial resolution of the HI survey is shown by the vertical long-dashed line. In the bottom panel, the solid line shows the predicted slope of –3.5, and the dashed line is a fit to the data, of -2.9 ± 1.4. Note that only the high-velocity tail of the distribution corresponds to the expanding shells; the remainder are near the sound speed, and in pressure equilibrium with the ambient ISM. (From Oey & Clarke 1998*b*.)

where R and P_i are, respectively, the superbubble radius and interior pressure, and n and t are the ambient ISM density and object age. These relations assume adiabatic evolution, namely, that the shells are pressure-driven by the shock-heated interior gas with no thermal losses.

For these simple analytic relations given by equations 4.1 – 4.3, Oey & Clarke (1997) derived global parameterizations of superbubble populations, assuming continuous or burst creation scenarios and that the shells stop growing when they are pressure-confined

by the ambient ISM. For example, it is straightforward to derive that the steady-state size distribution for the mechanical luminosity function in equation 4.1 and a continuous creation rate is,

$$N(R) \propto R^{-3}\, dR \quad . \tag{4.4}$$

At present, the only galaxies for which this prediction can be reliably tested are the LMC and SMC, both of which have deep HI surveys and shell catalogs. The top panel of Figure 6 shows the size distribution for SMC HI shell catalog (Staveley-Smith et al. 1997), which is in excellent agreement with the general prediction of equation 4.4 (Oey & Clarke 1997). The distribution in shell expansion velocities v, can be similarly derived for the same population parameterizations (Oey & Clarke 1998*b*):

$$N(v)\, dv \propto v^{-7/2}\, dv \quad . \tag{4.5}$$

The bottom panel of Figure 6 again shows agreement with this prediction for the SMC shells, for those objects that are still expanding (Oey & Clarke 1998*b*). On the other hand, the LMC shell population (Kim et al. 1999) is different in nature. Whereas the SMC catalog has > 500 distinct HI shells (Staveley-Smith et al. 1997), the LMC catalog has only 126 coherent objects, in a survey with similar instrumental sensitivities. Since the LMC is larger and has a substantially higher star formation rate than the SMC, the smaller shell population is at first sight counter-intuitive. However, as discussed below, the LMC's star-formation rate appears to be high enough that the shells frequently interact and merge, thereby losing their individual entities. Our predictions for the shell size distribution and other global parameters cannot apply in such circumstances.

4.2. *The Threshold SFR for Feedback to the IGM*

Indeed, we can derive a threshold star-formation rate (SFR) above which we expect this condition of shell interactions and ISM shredding. The porosity parameter Q is a conventional way to parameterize the hot (10^6 K) ionized medium (HIM) in galaxies. Q is essentially the filling factor of this hot gas, and, since it is thought to originate from shock-heating by SN explosions, Q can be estimated as the total volume of superbubbles relative to the relevant galaxy volume. For $Q > 1$, the galaxy is generating more hot gas than it can contain, and an outflow is predicted. This also implies that the neutral ISM is shredded, thereby allowing the escape of ionizing photons from the massive star population. Oey & Clarke (1997) derived specific relations for Q, for two- and three-dimensional situations, and Clarke & Oey (2002) derived the critical star-formation rate $\mathrm{SFR_{crit}}$ in general terms:

$$\mathrm{SFR_{crit}} = 0.15 \left(\frac{M_{\mathrm{ISM},10} \tilde{v}_{10}^2}{f_d} \right) \ \mathrm{M_\odot\ yr^{-1}} \quad , \tag{4.6}$$

where $M_{\mathrm{ISM},10}$ is the ISM mass in units of 10^{10} $\mathrm{M_\odot}$, $\tilde{v}_{10}$ is the ISM thermal velocity in units of 10 $\mathrm{km\,s^{-1}}$, and f_d is a geometric correction factor for disk galaxies.

For the Milky Way, Clarke & Oey (2002) found that $\mathrm{SFR_{crit}} \sim 1\ \mathrm{M_\odot\ yr^{-1}}$, similar to our Galaxy's estimated star-formation rate, and implying that it is close to this threshold. They also found that most local starburst galaxies might be expected to exceed this criterion, since they often have smaller $\mathrm{SFR_{crit}}$ but larger star-formation rates in comparison to our Galaxy. Lyman-break galaxies should also show escaping ionizing radiation. Note that the $\mathrm{SFR_{crit}}$ criterion is not based on an escape velocity, but rather an over-pressure.

A large sample of nearby galaxies that can be used to test this model is the Survey for Ionization in Neutral-Gas Galaxies (SINGG; Meurer et al. 2006), which is an Hα survey

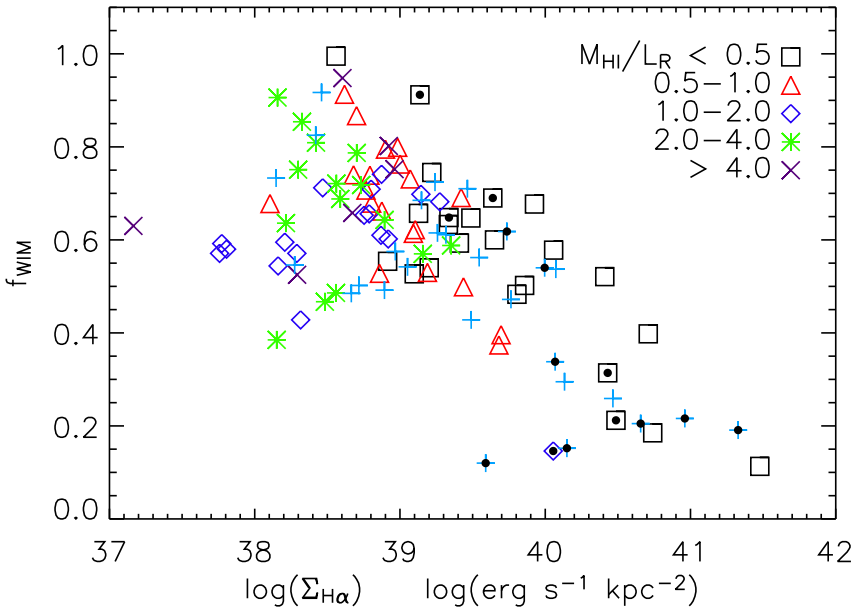

FIGURE 7. Fraction $f_{\rm WIM}$ of diffuse emission relative to total Hα luminosity for 109 galaxies from the SINGG survey as a function of Hα surface brightness $\Sigma_{\rm H\alpha}$, computed within the Hα half-light radius. Symbols are assigned by HI gas fraction $M_{\rm HI}/L_R$ as shown, and black dots indicate galaxies dominated by nuclear star formation. (From Oey *et al.* 2006.)

of an optically-blind, HI-selected galaxy sample. For the first dataset of 109 galaxies, we used the HIIphot software of Thilker et al. (2000) to define the boundaries of the classical HII regions, assigning all remaining Hα emission to the WIM. Figure 7 shows the WIM fraction $f_{\rm WIM}$ of the Hα emission vs the Hα surface brightness $\Sigma_{\rm H\alpha}$ for the sample. Galaxies with the highest $\Sigma_{\rm H\alpha}$ within the star-forming disk show the lowest $f_{\rm WIM}$. We refer to galaxies having $\Sigma_{\rm H\alpha} > 2.5\times10^{39}$ erg s^{-1} kpc^{-2} as "starburst" galaxies here, although Heckman (2005) defines starbursts as much more intense systems having $\Sigma_{\rm H\alpha} > 10^{41}$ erg s^{-1} kpc^{-2}. Figure 8 shows co-added Hα surface brightness distributions of galaxies in the SINGG sample, in three bins of $\Sigma_{\rm H\alpha}$. It is again apparent that our starburst galaxies have the flattest slope for the lowest surface brightnesses, also demonstrating that they have the lowest $f_{\rm WIM}$.

A possible cause for the lower Hα diffuse fraction in starbursts could be a lower fraction of ionizing field stars, as implied by equation 2.4. If this is the dominant effect, then we should similarly see it reflected in a relation between $f_{\rm WIM}$ and the total SFR as measured, for example, by the total Hα luminosity. However, Oey et al. (2006) show that such an effect is not seen, and thus, the lower fraction of field stars is not the dominant cause of the trend in Figure 7.

We do note that local starbursts are expected to exceed the SFR$_{\rm crit}$ threshold criterion for the escape of ionizing radiation (equation 4.6). Figure 7 shows that the galaxies with the lowest HI gas fractions, as measured by $M_{\rm HI}/L_R$, are those that most strongly exhibit the anti-correlation in $f_{\rm WIM}$ vs $\Sigma_{\rm H\alpha}$, with $M_{\rm HI}$ corresponding to the HI gas mass, and L_R to the R-band luminosity. The low HI gas fractions are consistent with a model in which there is not enough neutral gas for the total ionizing luminosity, and some of the

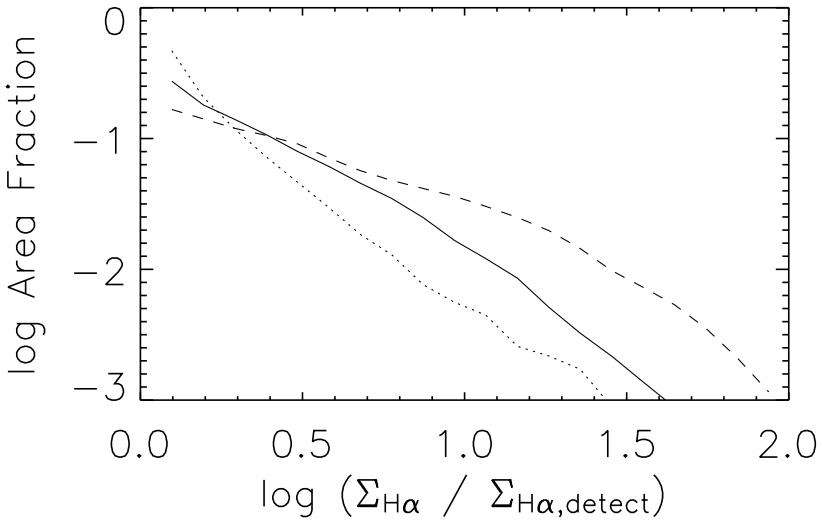

FIGURE 8. Co-added Hα surface brightness distributions for the SINGG galaxies. The dashed line shows "starburst" galaxies having log $\Sigma_{\rm H\alpha} > 39.7$, the solid line shows galaxies with $38.7 < \log \Sigma_{\rm H\alpha} \leqslant 39.7$, and the dotted line shows galaxies with log $\Sigma_{\rm H\alpha} \leqslant 38.7$; units of $\Sigma_{\rm H\alpha}$ are erg s^{-1} kpc^{-2}. Only pixels with a signal above a 3σ detection level are included. (From Oey *et al.* 2006.)

radiation is lost from these galaxies. Note that ionizing photons could be lost through the shredded geometry of the ISM, as suggested in the Clarke & Oey (2002) model, or the ISM could simply be fully ionized and density-bounded. Since neutral gas is detected in all of the galaxies, we favor the former model, but it may also be possible that the star-forming disk is fully ionized and that the unresolved HI detections result from the outer regions of the galaxies. Oey et al. (2006) present a more complete discussion, in which they show that a substantial fraction of the SINGG galaxies exceed the $\rm SFR_{crit}$ threshold for the escape of ionizing radiation, including all of the starburst galaxies. At the same time, they also show that the relation between $f_{\rm WIM}$ and $\Sigma_{\rm H\alpha}$ in Figure 7 is consistent with the simplest expectations for density-bounding. These results are strongly suggestive that ionizing radiation is escaping from starburst galaxies through at least one of these mechanisms. Nevertheless, we caution that several searches for Lyman continuum emission from galaxies have yielded negative results (e.g., Heckman et al. 2001; Leitherer et al. 1995); whereas more recently, the blue compact dwarf galaxy Haro 11 does show a detection (Bergvall et al. 2006), and at least two Lyman-break galaxies also show unambiguous Lyman continuum emission (Shapley et al. 2006). However, the positive detections correspond to low escape fractions ($\lesssim 5\%$) of the total ionizing radiation. Further studies are necessary to resolve these important and tantalizing issues regarding the Hα diffuse fraction and implied consequences.

5. Chemical Feedback

The third feedback process is the nucleosynthesis by massive stars and their core-collapse supernovae. The element enrichment of the ISM in galaxies and their environments drives the chemical evolution of galaxies and the cosmos. As another massive star

feedback process, chemical evolution can again be modeled with the same parameterizations for the massive star population and mechanical feedback processes. The supernova activity heats the coronal gas within superbubbles, which is the immediate medium into which the nucleosynthetic products are injected. The elements can mix and disperse efficiently within this hot gas (Oey 2003; Tenorio-Tagle 1996), but their dispersal into cooler environments is a complex and poorly understood process. Pioneering simulations of the mixing and dispersal process are only recently emerging (e.g., Balsara & Kim 2005; de Avillez & Mac Low 2003; see also Scalo & Elmegreen 2004).

Oey (2000, 2003) introduced a rudimentary analytic model for galactic chemical evolution that is based on the simple parameterizations above. The model assumes that the enrichment volume for an OB association scales directly with the SN-driven superbubble volume, with the former being the volume into which the SN products are uniformly diluted. The superbubble size distribution given by equation 4.4 can therefore be used to derive the relative metallicity distribution in the ISM for the ensemble of massive star clusters given by equation 2.3. Note that the largest volumes dilute the products to the lowest metallicities, and so Oey (2000) obtains:

$$N(Z) \propto Z^{-2}\ dZ \quad , \quad Z_{\rm min} < Z < Z_{\rm max} \quad . \tag{5.1}$$

where Z is the ISM metallicity, uniformly distributed within each enrichment volume. We impose the condition that no further dispersal of the elements occurs beyond these individual volumes. Thus, this represents an extreme inhomogeneous, no-mixing model, which can be contrasted to the opposite extreme of the pure, homogeneous Simple Model (Schmidt 1963; Pagel & Patchett 1975) that is used as the standard reference for most studies of galactic chemical evolution.

Assuming that subsequent generations of massive stars generate the same metallicity distribution (equation 5.1), we can model the enrichment process by progressively summing the metallicities as the volumes overlap. Thus, after n generations of star formation, the instantaneous metallicity distribution function (MDF) is given by,

$$N_{\rm inst}(Z) = \sum_{j=1}^{n}\ P_j\ N_j(Z) \quad . \tag{5.2}$$

where $N_j(Z)$ is the MDF for the ensemble of j overlapping volumes, which can be generated from the parent MDF given by equation 5.1. Note that any other form of the parent MDF can also be used in place of equation 5.1, and also that the Central Limit Theorem implies that $N_j(Z)$ approximates a Gaussian distribution in the limit of large j. P_j is the probability of obtaining j overlapping regions, and is given by the binomial distribution:

$$P_j = \binom{n}{j}\ Q^j\ (1-Q)^{n-j} \quad , \quad 1 \leqslant j \leqslant n \quad , \tag{5.3}$$

where Q is the volume filling factor, that is again simply scaled from the porosity parameter considered above.

Equation 5.2 therefore offers a Simple Inhomogeneous Model (SIM), which is in the spirit of the homogeneous, Simple Model, but which can be compared to observed *instantaneous* MDFs. The SIM is especially relevant to the most metal-poor systems, where stochastic effects dominate the evolution. It also emphasizes that the star-formation intensity, not merely the simple age of the system, is a major driver of the chemical evolution. The parameter that describes the evolutionary state in the SIM models is the product nQ, which is also the mean of the binomial distribution. Figure 9 shows a series of SIM models for different combinations of n and Q, with instantaneous MDFs shown

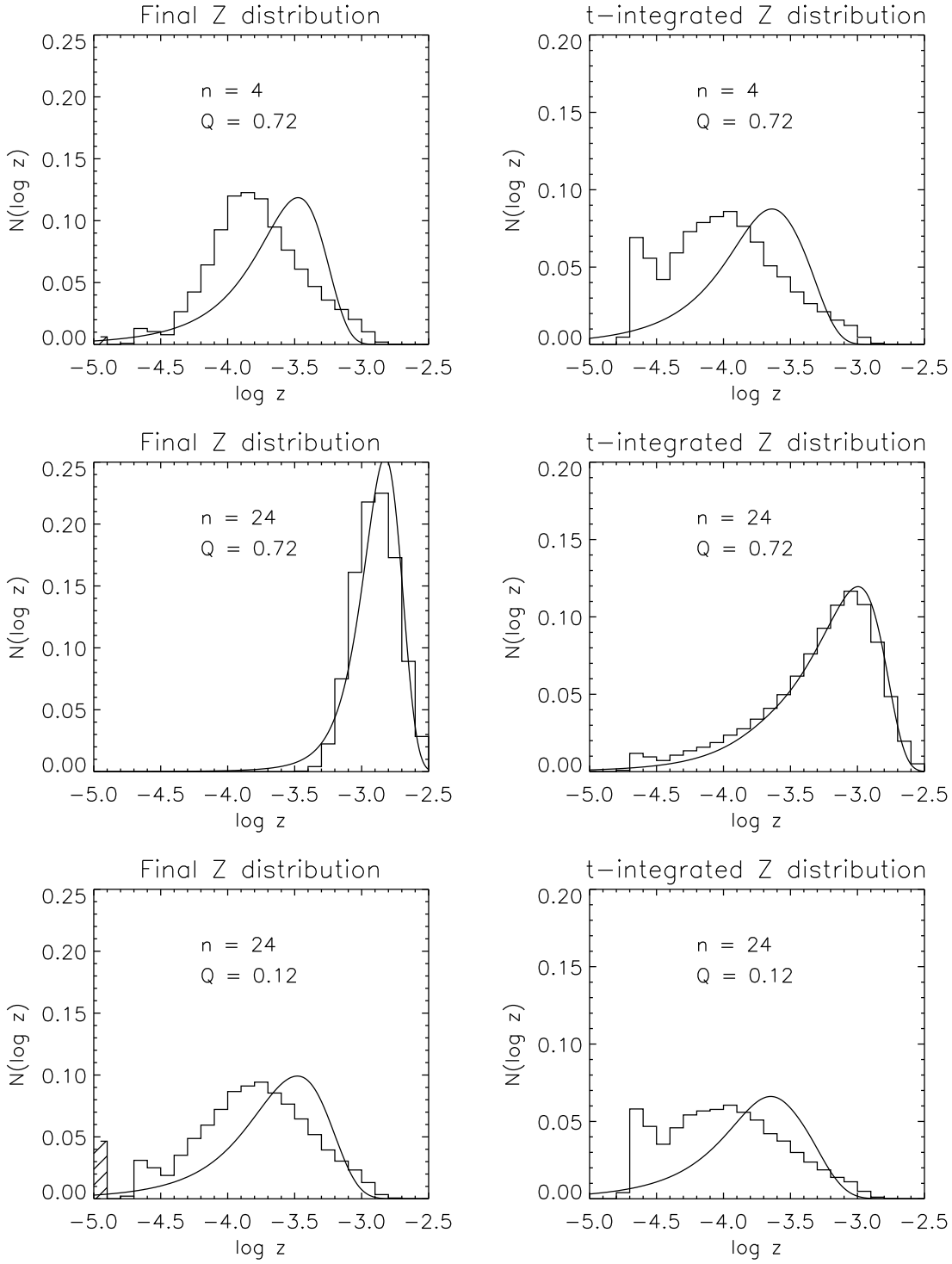

FIGURE 9. SIM models for different combinations of n and Q as shown, which correspond roughly to age and star-formation intensity, respectively. Final, instantaneous MDFs are shown on the left side, and the corresponding time-integrated MDFs are on the right. The SIM models are shown in the histograms, and analytic approximations, valid for large nQ, are shown by the curves.

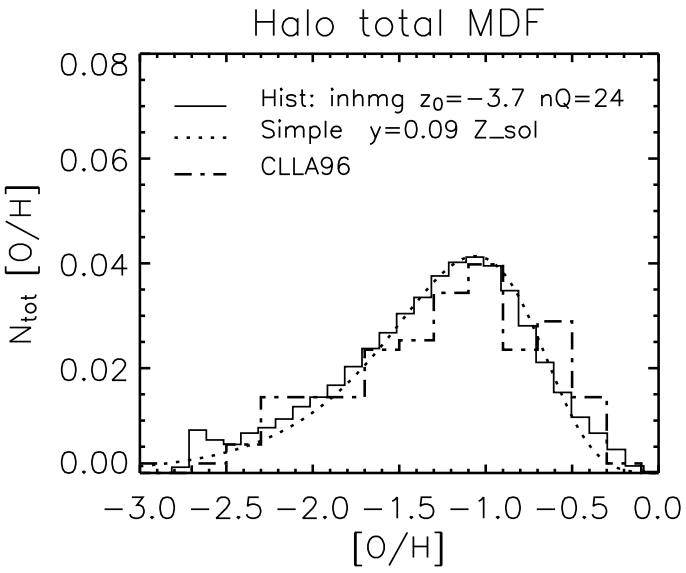

FIGURE 10. Halo metallicity distribution function converted to [O/H] from data by Carney *et al.* (1996, dot-dashed line). A Simple Inhomogeneous Model is overplotted with the solid line, and a homogeneous Simple Model is overplotted with the dotted line. The two models imply very different evolutionary states. (Based on Oey 2003.)

on the left. The right column shows corresponding models for time-integrated MDFs (see below). For the top and bottom models, the product nQ is the same, although the individual values of n and Q differ; we see that the resulting MDFs are qualitatively and quantitatively similar. In contrast, the middle panels show a model where the individual values of n and Q are the same as values in the top or bottom, yet the product nQ is much larger. For this model, the evolutionary state is much more evolved. Thus, an old system with a low star-formation intensity will have a similar MDF to a young system with a high star-formation intensity. This can straightforwardly explain the co-existence of old, metal-rich systems like the Galactic bulge, and extremely metal-poor systems like I Zw 18 that also show old stellar populations. These two systems may have similar ages, but extremely different time-integrated star-formation intensities, and they therefore show very different metallicities and evolutionary state, perhaps analogous to the middle and bottom models in Figure 9.

Oey (2000, 2003) also derived a cumulative, time-integrated MDF for all objects ever created out of the ISM whose enrichment proceeds in this way, namely, long-lived stars:

$$N_{\rm tot} = \frac{1}{n} \sum_{j=1}^{n} \sum_{k=j}^{n} D_{k-1}\ P_{j,k}\ N_j(Z) \tag{5.4}$$

We now include a depletion factor D_k, which is the fraction of gas remaining after k generations of star formation. Figure 10 compares the time-integrated SIM model (solid histogram) to the Galactic halo MDF from the data of Carney et al. (1996; dot-dashed). A homogeneous, Simple Model is also overplotted (dotted-line). We see that both models agree well with the data. However, Oey (2003) shows that the interpretations of these two models are extremely different: the Simple Model implies that the halo is a highly evolved system, because the decrease in high-metallicity stars is caused by a lack of remaining

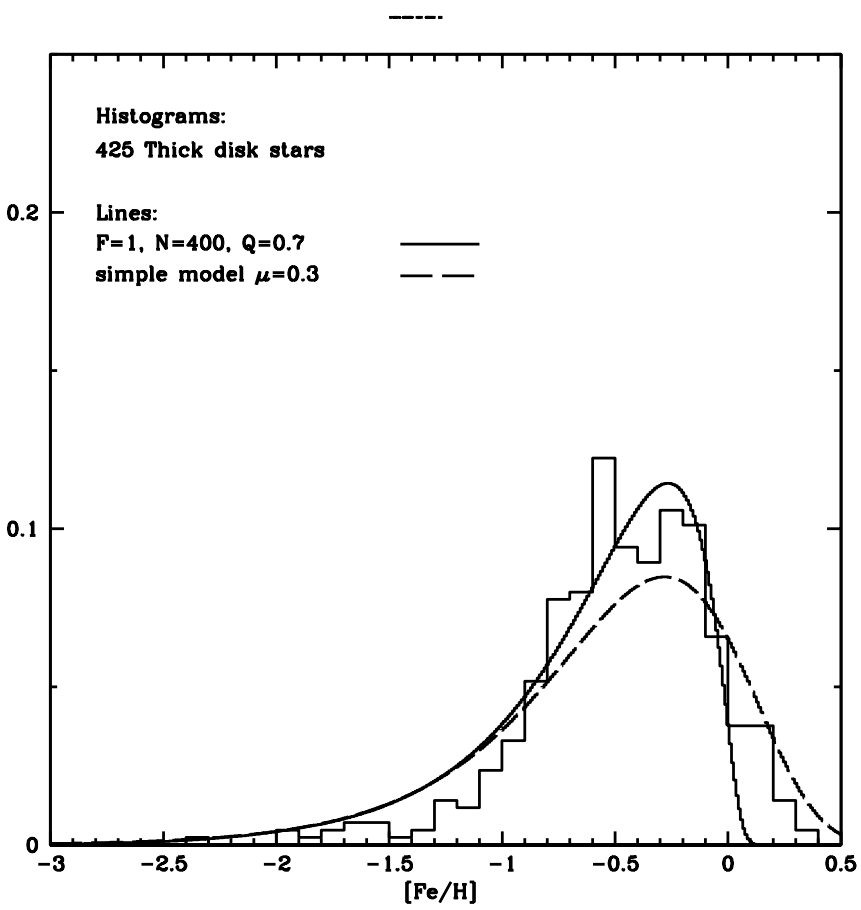

FIGURE 11. Metallicity distribution function for the Galactic thick disk from data by Nordström *et al.* (2004) and selection criteria of Bensby *et al.* (2003, 2005; solid histogram). The overplotted curves show a Simple Inhomogeneous Model (solid) and a Simple Model (dashed). (From Bensby & Oey 2006, in preparation.)

gas to form such stars. In contrast, the SIM implies that the halo is a relatively unevolved system, in which the decreasing high-metallicity tail is still dominated by the form of the parent MDF which is given by the Z^{-2} distribution (equation 5.1). Thus we see that further empirical constraints are necessary to distinguish between these dramatically different possibilities.

Real systems should follow evolution that is intermediate between these extremes described by the homogeneous Simple Model and inhomogeneous SIM. Figure 11 shows a preliminary MDF for the Galactic thick disk. The data correspond to F and G-dwarfs from the sample of Nordström et al. (2004), selected according to kinematic critera of Bensby et al. (2003, 2005). We overplot both a Simple Model (dashed line) and SIM model (solid line). We see that the thick disk data do in fact lie between the two models.

The only exception is in the low-metallicity tail, where the so-called G-dwarf Problem is seen: there is a lack of the lowest-metallicity stars, in comparison to both models, although the discrepancy is not as extreme as for the Galactic thin disk.

Another useful feature of the SIM model is that it offers a straightforward prediction for the fraction of zero-metallicity, Population III stars. For any given SIM model, it is simply the fraction of stars corresponding to $j = 1$, which do not overlap any preceding generations of contamination. Thus,

$$F_{\rm III} = \sum_{k=1}^{n} D_{k-1} P_{1,k} \Big/ \sum_{j=1}^{n} \sum_{k=j}^{n} D_{k-1} P_{j,k} \quad . \tag{5.5}$$

For the Galactic halo SIM model shown in Figure 10, $F_{\rm III} = 2 \times 10^{-2}$. As discussed by Oey (2003), this is two orders of magnitude below the empirical upper limit of 2×10^{-4}, demonstrating that the halo also shows a G-dwarf Problem, as also found by others (e.g., Prantzos 2003). Thus we see the power of these simple analytic models in raising fundamental issues regarding the formation and evolution of our Galaxy.

6. Summary

In summary, we see that empirical evidence thus far supports simple parameterizations of the massive star population in terms of their spatial distribution, given by the N_*^{-2} clustering law (equation 2.3), and mass distribution, given by a Salpeter (or similar) power-law IMF. The evidence is also suggestive, as described above, for a stellar upper-mass limit around 150 $M_\odot$, at least locally. The clustering law implies that about 10 – 30% of high-mass stars are field stars (equation 2.4), defined as those having no other massive star siblings in the host cluster. These simple parameterizations of massive stars as a population have powerful applications for analytically describing their feedback effects.

The ionizing radiation from these stars drives radiative feedback. The clustering law directly results in the HII region luminosity function, which shows a similar –2 power-law exponent, provided that the HII regions have enough ionizing stars to fully sample the stellar IMF. There is evidence that the upper limits to the HIILF vary across the Hubble Sequence, although the slope of the HIILF appears to be constant. Star-forming galaxies possess an ISM component at 10^4 K, which also appears to be ionized by the high-mass stellar population. Typically, about half of the total Hα emission from such galaxies is observed to originate from ordinary HII regions, while the remaining half originates from the diffuse, warm ionized medium. The diffuse WIM is likely ionized by both field stars and radiation escaping from the HII regions, in roughly equal parts. However, starburst galaxies show lower WIM fractions. The origin of this trend is unclear: data from the SINGG survey are consistent with predictions for escaping radiation based on shredding of the ISM by mechanical feedback; on the other hand, direct searches for Lyman continuum radiation from galaxies have shown extremely low ($\lesssim 5\%$) escape fractions.

The global mechanical feedback from the massive star population is dominated by their core-collapse SNe; stellar winds only play a significant role for the youngest populations, in which the highest mass stars remain unevolved and contribute the strongest stellar winds. In a steady-state scenario with constant global star-formation rate, the clustering law implies a resulting superbubble size distribution with a dependence of R^{-3} (equation 4.4) and expansion velocity distribution dependence of $v^{-7/2}$ (equation 4.5). These relations agree well for the HI shell catalog for the SMC. From the superbubble size

distribution, we can derive a galaxy's porosity parameter or volume filling factor for the superbubbles. This is a standard convention for estimating the magnitude of the hot (10^6 K) component of the ISM, which is thought to originate within the SN-heated interiors of the superbubbles. As the star-formation rate increases, the shells merge, shred the cooler ISM, and generate more hot gas than the galaxy can contain, thus driving a galactic outflow or superwind. It is possible to define a critical star-formation rate $\mathrm{SFR_{crit}}$, based on our previous parameterizations and ISM properties (equation 4.6); we find that it is on the order of a few $\mathrm{M_\odot\ yr^{-1}}$ for an L^* galaxy. We note that the LMC shows only 1/4 the total number of coherent HI shells compared to the SMC, despite its larger size and star-formation rate. This is consistent with the prediction that it is near $\mathrm{SFR_{crit}}$, so that the shells are merging and interacting. Thus, $\mathrm{SFR_{crit}}$ represents a threshold condition for the outflow of ionizing photons through the shredded ISM, as alluded to above, in addition to the outflow of hot gas and the newly-produced SN products. We note that this represents a pressure-driven model, independent of a galaxy's escape velocity.

The clustering law and resulting superbubble size distribution also offer a convenient framework for understanding the stochastic, inhomogeneous progression of galactic chemical evolution. Whereas the standard, Simple Model is purely homogeneous at all times, the Simple Inhomogeneous Model can make predictions for the *instantaneous* metallicity distribution function at any snapshot in time (equation 5.2). It can also predict cumulative MDFs (equation 5.4), and so it can also be applied to samples of long-lived stars. The SIM is applicable, in particular, to the most metal-poor conditions, and it agrees well with the Galactic halo metallicity distribution. This offers an alternative interpretation of the halo as a relatively unevolved population, in contrast to the highly-evolved status implied by the Simple Model. The SIM also offers an opposite extreme to the homogeneous Simple Model, within which observations may be bracketed. In addition, it emphasizes that a system's evolutionary status depends as much on the star-formation intensity, as on mere age. Finally, the SIM provides simple, straightforward predictions for the fraction of zero-metallicity, Population III stars for any given model (equation 5.5). Those for the Galactic halo confirm a discrepancy of at least two orders of magnitude in the observed lack of zero-metallicity stars compared to predicted fraction.

These diverse, massive-star feedback effects are all unified by the same set of analytic parameterizations for this energetic stellar population. The observations are largely, and remarkably, consistent across varying physical phenomena over an extreme range in scale and age. Thus, this simple, self-consistent framework offers powerful tools and insight on the role of the massive star population in the cosmos.

MSO thanks the Symposium organizers for their hospitality and travel support. Some of this work was supported by the National Science Foundation, grants AST-0448893 and AST-0448900; and the NASA Astrophysics Data Program, grant NAG5-10768.

REFERENCES

Baldry, I. K. & Glazebrook, K. 2003, *ApJ* 593, 258.
Banfi, M., Rampazzo, R., Chincarini, G., & Henry, R. B. C. 1993, *A&A* 280, 373.
Balsara, D. S. & Kim, J. 2005, *ApJ* 634, 390.
Bell, E. F. & de Jong, R. S. 2001, *ApJ* 550, 212.
Bensby, T., Feltzing, S., & Lundström, I. 2003, *A&A* 410, 527.
Bensby, T., Feltzing, S., Lundström, I., & Ilyin, I. 2005, *A&A* 433, 185.
Bergvall, N., Zackrisson, E., Andersson, B.-G., Arnberg, D., Masegosa, J., & Östlin, G. 2006, *A&A* in press; astro-ph/0601608.

Bonnell, I. A., Bate, M. R., & Zinnecker, H. 1998, *MNRAS* 298, 93.
Caldwell, N., Kennicutt, R., Phillips, A. C., & Schommer, R. A. 1991, *ApJ* 370, 526.
Carney, B. W., Laird, J. B., Latham, D. W., & Aguilar, L. A. 1996, *AJ* 112, 668.
Clarke, C. J. & Oey, M. S. 2002, *MNRAS* 337, 1299.
de Avillez, M. & Mac Low, M.-M. 2002, *ApJ* 581, 1047.
Elmegreen, B. G. 2000, *ApJ* 539, 342.
Elmegreen, B. G. 2006, *ApJ* in press; astro-ph/0605520.
Elmegreen, B. G. & Efremov, Y. N. 1997, *ApJ* 480, 235.
Elmgreen, B. G. & Lada, C. 1977, *ApJ* 214, 725.
Fernandes, I. F., de Carvalho, R., Contini, T., & Gal, R. R. 2004, *MNRAS* 355, 728.
Ferguson, A. M. N., Wyse, R. F. G., Gallagher, J. S., & Hunter, D. A., 1996, *AJ* 111, 2265.
Figer, D. F. 2005, *Nature* 434, 192.
Heckman, T. M. 2005, in *Starbursts: From 30 Doradus to Lyman Break Galaxies,* (eds.) R. de Grijs & R. M. González Delgado, *Ap&SS Library*, 329, 3.
Heckman, T. M., Sembach, K. R., Meurer, G. R., Leitherer, C., Calzetti, D., & Martin, C. L. 2001, *ApJ* 558, 56.
Hoopes, C. G. & Walterbos, R. A. M. 2000, *ApJ* 541, 597
Hunter, D. A., Vacca, W. D., Massey, P., Lynds, R., & O'Neil, E. J. 1997, *AJ* 113, 1691.
Hunter, D. A., Elmegreen, B. G., Dupuy, T. J., & Mortonson, M. 2003, *AJ* 126, 1836.
Kahn, F. D. 1974, *A&A* 37, 149.
Kennicutt, R. C., Edgar, B. K.., & Hodge, P. W. 1989, *ApJ* 337, 761.
Kim, S., Dopita, M. A., Staveley-Smith, L., & Bessell, M. S. 1999, *AJ* 118, 2797.
Koen, C. 2006, *MNRAS* 365, 590.
Kroupa, P. & Weidner C. 2003, *ApJ* 598, 1076.
Larson, R. B. & Starrfield, S. 1971, *A&A* 13, 190.
Ledoux, P. 1941, *ApJ* 94, 537.
Leitherer, C., Ferguson, H. C., Heckman, T. M., & Lowenthal, J. 1995, *ApJ* 454, L19.
Martins, F., Schaerer, D., & Hillier, D. J. 2005, *A&A* 436, 1049.
Massey, P., 2002, *ApJS* 141, 81.
Massey, P. 2003, *ARAA* 41, 15.
Massey, P. & Hunter, D. A. 1998, *ApJ* 493, 180.
Massey, P., Johnson, K. E., & DeGioia-Eastwood, K. 1995, *ApJ* 454, 151.
McCray R. & Kafatos M. 1987, *ApJ* 317, 190.
Meurer, G. R., et al. 2006, *ApJ* in press; astro-ph/0604444.
Meurer, G. R., Heckman, T. M., Leitherer, C., Kinney, A., Robert, C., & Garnett, D. R. 1995, *AJ* 110, 2665.
Nordström, B., *et al.* 2004, *A&A* 418, 989.
Oey, M. S. 2000, *ApJ* 542, L25.
Oey, M. S. 2003, *MNRAS* 339, 849.
Oey, M. S. *et al.* 2006, *ApJ* submitted.
Oey, M. S. & Clarke, C. J. 2005, *ApJ* 620, L43.
Oey, M. S. & Clarke, C. J. 1997, *MNRAS* 289, 570.
Oey, M. S. & Clarke, C. J. 1998*a*, *AJ* 115, 1543
Oey, M. S. & Clarke, C. J. 1998*b*, in *Interstellar Turbulence,* eds. J. Franco & A. Carramiñana, (Cambridge: Cambridge U. Press), 112.
Oey, M. S. & Kennicutt, R. C. 1997, *MNRAS* 291, 827.
Oey, M. S., King, N. L., & Parker, J. W. 2004, *AJ* 127, 1632.
Pagel, B. E. J. & Patchett, B. E. 1975, *MNRAS* 172, 13.
Parker, J. W., *et al.* 1998, *AJ* 116, 180.
Prantzos, N. 2003, *A&A* 404, 211.
Rand, R. J. 1992, *AJ* 103, 815.
Rand, R. J. 2000, *ApJ* 537, L13.
Repolust, T., Puls, J., & Herrero, A. 2004, *A&A* 415, 349.

Reynolds R. J. 1984, *ApJ* 282, 191.
Reynolds, R. J., Haffner, L. M., & Tufte, S. L., 1999, *ApJ* 525, L21.
Rozas, M., Beckman, J. E., & Knapen, J. H. 1996, *A&A* 307, 735.
Salpeter, E. E. 1955, *ApJ* 121, 161.
Scalo, J. & Elmegreen, B. G. 2004, *ARAA* 42, 275.
Scharzschild, M. & Härm, R. 1959, *ApJ* 129, 637.
Schmidt, M. 1963, *ApJ* 137, 758.
Selman, F., Melnick, J., Bosch, G., & Terlevich, R. 1999*a*, *A&A* 341, 98
Selman, F., Melnick, J., Bosch, G., & Terlevich, R. 1999*b*, *A&A* 347, 532.
Shapley, A. E., Steidel, C. C., Pettini, M., Adelberger, K. L., & Erb, D. K. 2006, *ApJ* in press; astro-ph/0606635.
Smith, L. J., Norris, R. P. F., & Crowther, P. A. 2002, *MNRAS* 337, 1309.
Staveley-Smith L., Sault R. J., Hatzidimitriou D., Kesteven M. J., McConnell D. 1997, *MNRAS* 289, 225
Stothers, R. B. 1992, *ApJ* 392, 706
Tenorio-Tagle, G. 1996, *AJ* 111, 1641.
Thilker, D. A., Braun, R., & Walterbos, R. A. M., 2000, *AJ* , 120, 3070
Voges, E. S., Walterbos, R. A. M., Hoopes, C. G., & Oey, M. S. 2005, in *Extra-Planar Gas,* ed. R. Braun, ASP Conf. Series 331, 225.
Walterbos, R. A. M., 1998, *PASA*, 15, 99.
Weaver R., McCray R., Castor J., Shapiro P., Moore R. 1977, *ApJ* 218, 377.
Weidner, C. & Kroupa, P. 2004, *MNRAS* 348, 187.
Wolfire, M. G. & Cassinelli, J. P. 1987, *ApJ* 319, 850.
Zhang, Q. & Fall, S. M. 1999, *ApJ* 527, L81.

Massive Stars: From Pop III and GRBs to the Milky Way, 2006 STScI May Symposium, eds. M. Livio et al., (Cambridge: Cambridge U. Press)